A Next-Generation BRAF Inhibitor Overcomes Resistance to BRAF Inhibition in Patients with *BRAF*-Mutant Cancers Using Pharmacokinetics-Informed Dose Escalation

Rona Yaeger[1], Meredith A. McKean[2], Rizwan Haq[3], J. Thaddeus Beck[4], Matthew H. Taylor[5], Jonathan E. Cohen[6], Daniel W. Bowles[7], Shirish M. Gadgeel[8], Catalin Mihalcioiu[9], Kyriakos P. Papadopoulos[10], Eli L. Diamond[1], Keren B. Sturtz[11], Gang Feng[12], Stefanie K. Drescher[11], Micaela B. Reddy[11], Bhaswati Sengupta[11], Arnab K. Maity[12], Suzy A. Brown[11], Anurag Singh[11], Eric N. Brown[11], Brian R. Baer[11], Jim Wong[11], Tung-Chung Mou[11], Wen-I Wu[11], Dean R. Kahn[11], Sunyana Gadal[1], Neal Rosen[1], John J. Gaudino[11], Patrice A. Lee[11], Dylan P. Hartley[11], and S. Michael Rothenberg[11,13]

ABSTRACT

RAF inhibitors have transformed treatment for patients with *BRAF*^{V600}-mutant cancers, but clinical benefit is limited by adaptive induction of ERK signaling, genetic alterations that induce *BRAF*^{V600} dimerization, and poor brain penetration. Next-generation pan-RAF dimer inhibitors are limited by a narrow therapeutic index. PF-07799933 (ARRY-440) is a brain-penetrant, selective, pan-mutant BRAF inhibitor. PF-07799933 inhibited signaling *in vitro*, disrupted endogenous mutant-BRAF:wild-type-CRAF dimers, and spared wild-type ERK signaling. PF-07799933 ± binimetinib inhibited growth of mouse xenograft tumors driven by mutant *BRAF* that functions as dimers and by *BRAF*^{V600E} with acquired resistance to current RAF inhibitors. We treated patients with treatment-refractory *BRAF*-mutant solid tumors in a first-in-human clinical trial (NCT05355701) that utilized a novel, flexible, pharmacokinetics-informed dose escalation design that allowed rapid achievement of PF-07799933 efficacious concentrations. PF-07799933 ± binimetinib was well-tolerated and resulted in multiple confirmed responses, systemically and in the brain, in patients with *BRAF*-mutant cancer who were refractory to approved RAF inhibitors.

SIGNIFICANCE: PF-07799933 treatment was associated with antitumor activity against *BRAF*^{V600}- and non-V600-mutant cancers preclinically and in treatment-refractory patients, and PF-07799933 could be safely combined with a MEK inhibitor. The novel, rapid pharmacokinetics (PK)-informed dose escalation design provides a new paradigm for accelerating the testing of next-generation targeted therapies early in clinical development.

[1]Memorial Sloan Kettering Cancer Center, New York, New York. [2]Sarah Cannon Research Institute, Nashville, Tennessee. [3]Dana Farber Cancer Institute, Boston, Massachusetts. [4]Highlands Oncology, Fayetteville, Arkansas. [5]Earle A. Chiles Research Institute, Providence Cancer Institute, Portland, Oregon. [6]Hadassah Medical Center, Jerusalem, Israel. [7]University of Colorado Hospital, Aurora, Colorado. [8]Henry Ford Health System, Detroit, Michigan. [9]McGill University Health Centre, Montreal, Canada. [10]South Texas Accelerated Research Therapeutics, San Antonio, Texas. [11]Pfizer Boulder Research and Development, Boulder, Colorado. [12]Pfizer Early Clinical Development, Cambridge, Massachusetts. [13]Pfizer Oncology Research and Development, La Jolla, California.

Corresponding Authors: Rona Yaeger, Department of Medicine, Memorial Sloan Kettering Cancer Center, New York, NY 10065. E-mail: yaegerr@mskcc.org; and S.M. Rothenberg, insitro inc., South San Francisco, CA 94080. E-mail: smichael@insitro.com

Cancer Discov 2024;14:1599–611

doi: 10.1158/2159-8290.CD-24-0024

INTRODUCTION

Oncogenic *BRAF* mutant protein monomers are categorized into Class I (monomers), II (RAS-independent, constitutively activated dimers), and III (RAS-dependent, hypoactive dimers) based on their activities as monomers or homo/heterodimers (1, 2). Approved RAF kinase inhibitors are potent against Class I $BRAF^{V600}$ mutants, which function as monomers. Despite effective immediate pathway suppression, long-term benefit is limited by several potential mechanisms: (i) adaptive induction of ERK signaling, (ii) clinical resistance most commonly arising from new genetic alterations that induce BRAF dimerization, and (iii) poor brain penetration enabling intracranial disease progression. In addition, approved RAF inhibitors cause paradoxical activation of ERK signaling in *BRAF* wild-type cells, allowing combination with MEK or EGFR inhibitors to both mitigate the resulting on-target toxicities and improve efficacy. However, the combination partners introduce additional toxicities, and resistance remains universal. Genetic causes of resistance are best understood in melanoma and largely converge on the development of RAF dimers. Resistance alterations include dimer-inducing *BRAF* splice variants, *BRAF* gene amplification, and *RAS* mutations in the setting of founder $BRAF^{V600}$ mutations. Further, non-V600 dimer-forming *BRAF* Class II/III founder mutations (including fusions) have been identified in ~4% to 8% of all solid tumors (3–13).

Next-generation RAF inhibitors have been developed with the goal of inhibiting ERK activation by *BRAF* mutants that form dimers as well as monomers. Many are pan-RAF dimer inhibitors that preclinically inhibit signaling from not only *BRAF* mutants but also all three wild-type RAF proteins. However, emerging clinical data demonstrate that efficacy is limited by on-target toxicity from pan-wild-type RAF inhibition, which limits combinability with MEK inhibitors and requires both intermittent dosing and dose modifications (14–19).

Selective inhibitors of BRAF-containing dimers such as plixorafenib (PLX-8394, FORE8394) also maintain activity against *BRAF* mutants, including V600 and non-V600 mutants (20). Because such compounds also spare CRAF homodimers and ARAF-containing dimers, they have the advantage of maintaining MAPK signaling in normal tissue. However, plixorafenib is subject to CYP3A4-dependent metabolism, thus requiring coadministration with the CYP3A inhibitor cobicistat to reach efficacious exposure (21). Furthermore, cobicistat cotreatment unfavorably increases hepatotoxicity and hampers rational combinations with MEK inhibitors, many of which are CYP3A4 substrates (22, 23).

PF-07799933 (ARRY-440) is a next-generation, selective pan-mutant BRAF inhibitor that is not a pan-RAF inhibitor, does not possess the metabolic liability of plixorafenib, can be combined with MEK inhibitors, and is brain-penetrant. Given the significant unmet need faced by patients with *BRAF*-mutant cancers after the failure of available treatments, we aimed to implement a data-informed dose escalation approach in the first-in-human phase 1 trial to achieve therapeutic exposures in less time and with fewer patients overall.

RESULTS

PF-07799933 Disrupts Mutant *BRAF* Dimers to Overcome Diverse *BRAF* Mutants Preclinically

PF-07799933 (ARRY-440), an orthosteric, pan-mutant BRAF inhibitor, was discovered by Array BioPharma. We profiled PF-07799933 and three classes of BRAF inhibitors—BRAF V600 monomer inhibitor (encorafenib), selective BRAF dimer inhibitor (plixorafenib), and pan-RAF dimer inhibitors (belvarafenib, tovorafenib, naporafenib, and exarafenib)—in 1-hour assays of phosphorylated ERK (pERK), across 19 patient-derived cancer cell lines (20, 24–27). These lines were *BRAF* wild-type or harbored founder mutations in *BRAF*, including Class I (i.e., V600E/K), Class II (i.e., L597V/R and G469A), or Class III (i.e., G466V and D594G) alterations (1, 2), and indels (V487-P492, N486-P490, and L485-P490) with a different mechanism of activation (28, 29). We also included two $BRAF^{V600E}$-mutant melanoma cell lines harboring commonly occurring acquired resistance alterations identified in patients with melanoma after treatment with approved BRAF inhibitors: *BRAF* splice variant (p61) or *RAS* mutation (*NRAS*-Q61K; Supplementary Table S1 summarizes each cell line with its specific *BRAF* mutation; refs. 3, 4).

PF-07799933 demonstrated broad inhibition of pERK levels in cell lines harboring Class I (IC_{50} = 0.7–7 nmol/L), II (10–14 nmol/L), III (0.8–7.8 nmol/L), and indel (113–179 nmol/L) mutants, acquired *BRAF* p61 splice variant (59 nmol/L), and acquired $NRAS^{Q61K}$ (16 nmol/L), but significantly spared pERK in *BRAF* wild-type cells (≥9,800 nmol/L; Fig. 1A). Unsupervised hierarchical clustering demonstrated that PF-07799933 was most similar to plixorafenib, though with better potency. Encorafenib occupied a distinct branch, with more pERK inhibitory activity against Class I *BRAF*-mutant cell lines (IC50 = 3.4–58 nmol/L) than cell lines with Class II (40–2,700 nmol/L), Class III (308–990 nmol/L), indel (6.2–154 nmol/L), $BRAF^{V600E}$ + p61 splice variant (322 nmol/L), or $BRAF^{V600E}$ + $NRAS^{Q61K}$ (172 nmol/L) mutant cell lines. Pan-RAF dimer inhibitors clustered together based on similar response profiles across the cell lines evaluated, with similar pERK inhibitory activity against wild-type and mutant *BRAF*. In *BRAF* wild-type cells, PF-07799933 demonstrated no pERK inhibition, in contrast to the pan-RAF dimer inhibitors, and less paradoxical activation of pERK than encorafenib (Fig. 1A; Supplementary Fig. S1A). Isothermal stability shift dose–response assays (ITDR) showed that PF-07799933 bound $BRAF^{V600E}$ with a 10-fold higher affinity compared with wild-type CRAF protein in A375 $BRAF^{V600E}$-mutant melanoma cell lysates (Supplementary Fig. S1B).

To gain insight into the mechanism of mutant *BRAF* inhibition by PF-07799933, we immunoprecipitated endogenous BRAF/CRAF protein complexes with either BRAF- or CRAF-specific antibodies, in two $BRAF^{V600E}$-mutant melanoma cell lines with an acquired *BRAF* p61 splice variant (in cis with the *de novo* V600E allele; Fig. 1B) or with $NRAS^{Q61K}$ (Supplementary Fig. S1C), both of which promote mutant BRAF-dimer formation. As previously described, the approved BRAF monomer inhibitor encorafenib increased mutant-*BRAF*:wild-type-*CRAF* complexes in a dose-dependent manner (Fig. 1B; Supplementary Fig. S1C; refs. 30–32).

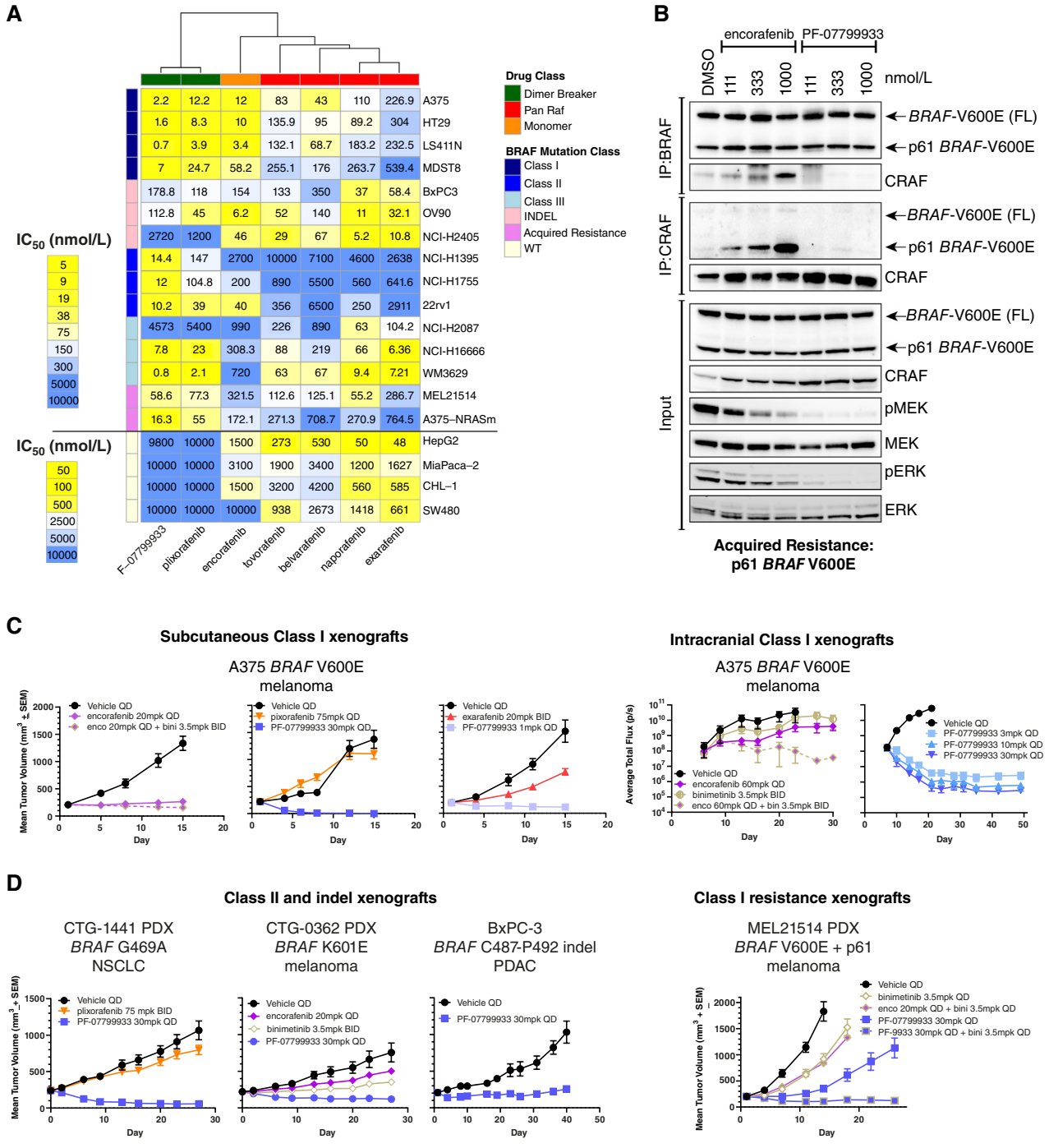

Figure 1. Preclinical characterization of pan-mutant BRAF selective monomer/dimer inhibitor PF-07799933. **A,** Heatmap of 50% inhibitory concentration (IC_{50}) values for inhibition of pERK in human cancer cell lines for PF-07799933 and comparator RAF inhibitors, as derived from dose–response curves in Supplementary Fig. S1. Each cell line with specific *BRAF* mutation is summarized in Supplementary Table S1. Note color scaling for *BRAF* wild-type cell lines is distinct from *BRAF*-mutant cell lines. Unsupervised clustering of compounds is shown using Euclidean distance as a similarity metric. **B,** Immunoprecipitation of BRAF and CRAF dimer complexes in the MEL21514 (p61 *BRAF* splice variant) melanoma cell line. Comparison of dimer-breaking effects of PF-07799933 and encorafenib are shown at indicated drug concentrations for a 1-hour incubation period. **C,** Efficacy curves of mean tumor volumes in mice ($n = 8$–10) bearing subcutaneous xenografts (left) and change in flux measurements of intracranial xenografts (right) of Class I A375 ($BRAF^{V600E}$) melanoma cells following oral treatment with the indicated agents. **D,** Efficacy curves of mean tumor volumes in mice ($n = 8$–10) bearing subcutaneous patient-derived or cell line xenografts of Class II, indel, and Class I acquired resistance models following oral treatment with the indicated agents. IC_{50}, 50% inhibitory concentration; nM, nanomolar; INDEL, insertion/deletion; WT, wild-type; IP, immunoprecipitated; FL, full-length; mm^3, cubic millimeter; SEM, standard error of mean; QD, once daily; BID, twice daily; mpk, milligrams per kilogram; NSCLC, non–small cell lung cancer; PDAC, pancreatic adenocarcinoma.

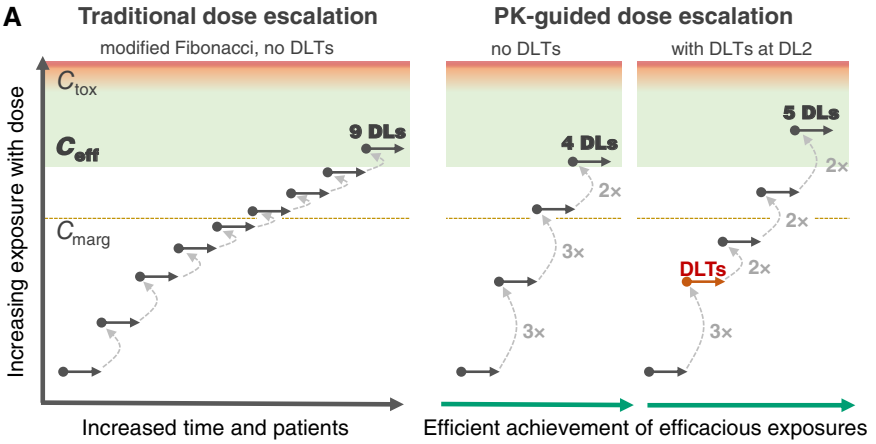

B

PF-07799933 monotherapy dose escalation PK

DL | dose | Pt	AUC_{tau}, µg/mL*h	C_{max}, µg/mL	MOE AUC_{tau}	MOE C_{max}	DLTs	Dose escalation
STD_{10} rat	4040	197				
DL1 | 50 mg QD | 1	17.9	1.90	**226**	**104**	0	
DL1 | 50 mg QD | 2	Not evaluable	1.36	**—**	**145**	0	**3-fold**
DL1 | 50 mg QD | 3	21.0	1.78	**192**	**111**	0	
DL2 | 150 mg QD | 1	30.1	1.77	**134**	**111**	0	
DL2 | 150 mg QD | 2	87.9	4.23	**46**	**47**	0	**3-fold**
DL2 | 150 mg QD | 3	104	5.82	**39**	**34**	0	
DL3 | 225 mg BID | 1	166	15.9	**24**	**12**	0	
DL3 | 225 mg BID | 2	493	52.7	**8**	**4**	0	**2-fold**
DL3 | 225 mg BID | 3	199	19.9	**20**	**10**	0	

C

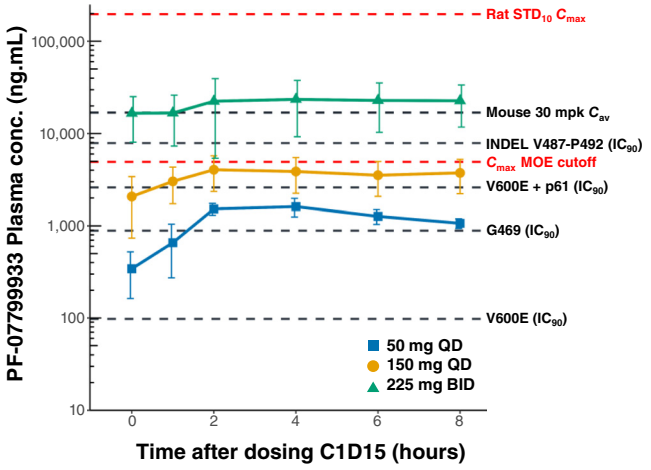

Figure 2. PF-07799933 safety and rapid PK-guided dose escalation. **A,** Examples of traditional (left) vs. PK-guided dose escalation (right) for a drug with a wide therapeutic index based on preclinical data and available clinical data for similar drugs. With traditional dose escalation (example of modified Fibonacci dose escalation design with decreasing dose increments at higher dose levels), even without DLTs, it can require many dose levels and patients to reach a potentially efficacious exposure (C_{eff}). In contrast, PK-guided dose escalation may require fewer dose levels, time, and patients to reach a potentially efficacious exposure. An example shown is a threefold dose increase in the absence of DLTs and if drug exposures are lower than the potentially toxic exposure (C_{tox}) by at least a prespecified safety margin (C_{marg}); otherwise, a twofold dose increase. **B,** Preliminary C_{max}, AUC_{tau}, and MOE values for each patient on Cycle 1 Day 15 (C1D15) of dosing for patients with available PK at the time of dose escalation. At a given dose level, if MOEs (rat value at STD_{10}/human value for C_{max} and AUC_{tau}) are >40 in at least two out of three participants, and no DLTs are observed at the current and all prior dose levels, a threefold dose increase is allowed; otherwise, the maximum dose increase is twofold. **C,** Preliminary plasma concentration vs. time data (mean ± standard deviation for $n = 3$–5 per dose level) on C1D15. Horizontal reference lines show plasma concentrations for IC_{90} *BRAF*-mutant protein target coverage based on the cell-based pERK assay, the average concentration (C_{av}) in the mouse xenograft at a 30-mg/kg dose (shown to be efficacious for multiple tumor types), the C_{max} at the rat (sensitive tox species) STD_{10} and the C_{max} at the cutoff allowing a threefold dose increase (i.e., C_{max}/40). To enroll patients with symptomatic brain metastases, C_{trough} on C1D15 had to exceed the G469A IC_{90} in at least one-half of patients, achieved at 150 mg QD. PK, pharmacokinetics; DLT, dose-limiting toxicity; DL, dose level; PT, patient; AUC_{tau}, area under the dose–response curve to end of dosing interval; MOE, margin of exposure; mg, milligrams; QD, daily; BID, twice daily; ng, nanograms; conc, concentration; ml, milliliters; STD_{10}, severely toxic dose in 10% animals; mpk, milligrams per kilogram; C_{av}, average concentration; C_{max}, maximum concentration; IC_{90}, 90% inhibitory concentration.

In contrast, heterodimeric complexes containing wild-type *CRAF* with *BRAF*^{V600E} or the *BRAF*^{V600E}; p61 splice variant were disrupted by PF-07799933 (Fig. 1B; Supplementary Fig. S1C). Notably, PF-07799933 failed to disrupt wild-type-*BRAF*:wild-type-*CRAF* dimer complexes in *BRAF* wild-type cells with exogenously expressed wild-type *BRAF* and wild-type *CRAF* (Supplementary Fig. S1D). The ability to break endogenous, mutant-*BRAF*:wild-type-*CRAF* dimers without disrupting wild-type-*BRAF*:wild-type-*CRAF* dimers contributes to the enhanced potency, efficacy, and safety of PF-07799933.

We also solved the cocrystal structures of the BRAF kinase domain with encorafenib and PF-07799933 (Supplementary Fig. S2A and S2B; Supplementary Table S2). Compared with encorafenib, PF-07799933 induced an ordered A-loop and caused an outward rotation in the αC-helix, both consistent with an inactive kinase conformation that may destabilize RAF dimers or prevent dimerization and reduce RAF affinity to MEK due to conformational hindrance. Based on published structures of RAF kinases, plixorafenib may also change the position of the αC-helix to disrupt select dimers (20).

In vivo antitumor activity was assessed in mouse xenografts harboring representative *BRAF* mutations and treated orally with different agents at doses selected to approximate the clinically achievable human exposures (when human data were available). PF-07799933 monotherapy drove deeper regressions than encorafenib + binimetinib in mouse xenografts harboring the founder *BRAF*^{V600E} (Class I) mutation implanted subcutaneously [Fig. 1C (left)] or intracranially [Fig. 1C

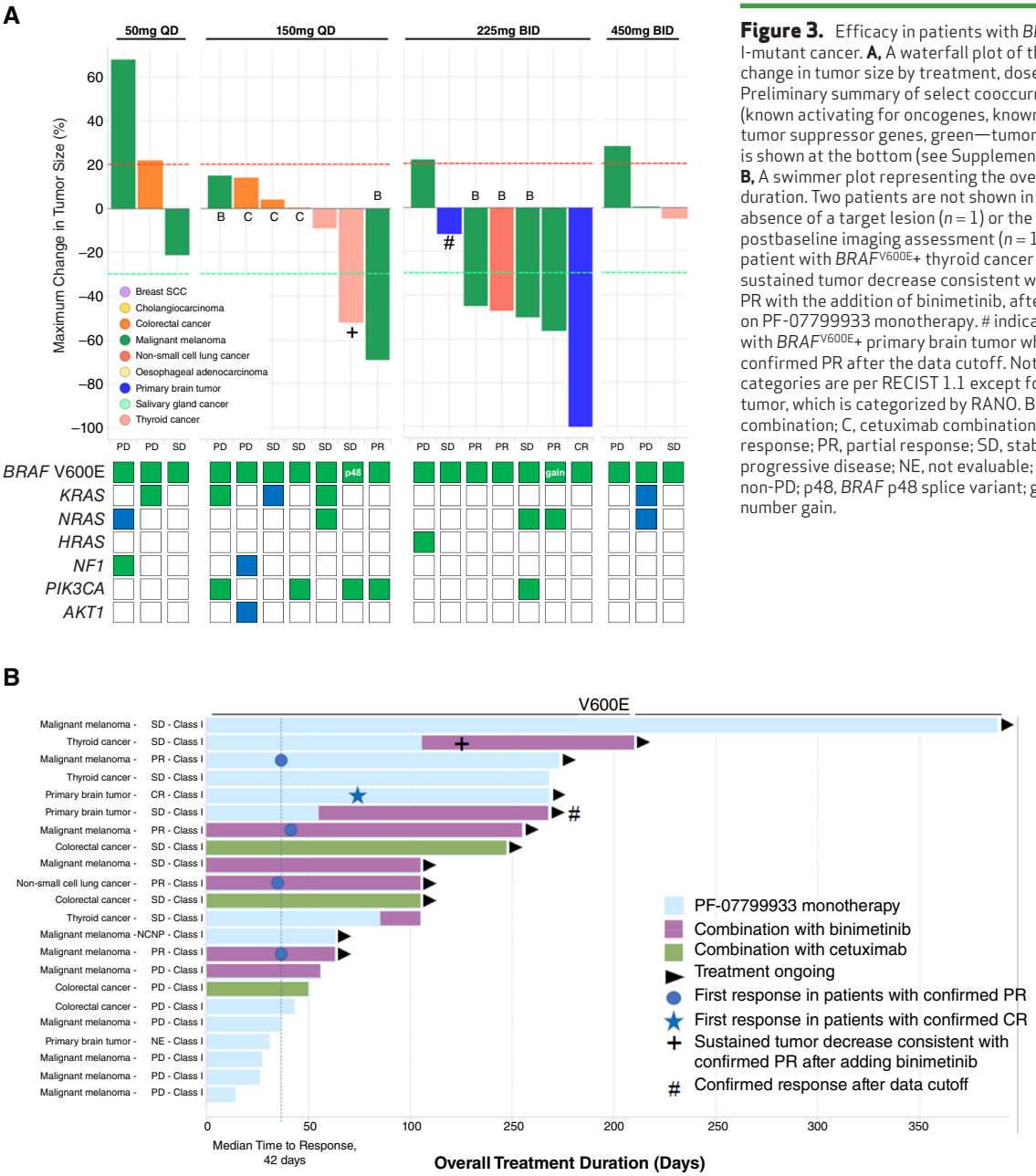

Figure 3. Efficacy in patients with *BRAF*^{V600E}/Class I-mutant cancer. **A,** A waterfall plot of the maximum change in tumor size by treatment, dose, and tumor. Preliminary summary of select cooccurring mutations (known activating for oncogenes, known inactivating for tumor suppressor genes, green—tumor, blue—ctDNA) is shown at the bottom (see Supplementary Table S5). **B,** A swimmer plot representing the overall treatment duration. Two patients are not shown in **A** due to the absence of a target lesion ($n = 1$) or the absence of postbaseline imaging assessment ($n = 1$). + indicates patient with *BRAF*^{V600E}+ thyroid cancer who achieved sustained tumor decrease consistent with a confirmed PR with the addition of binimetinib, after progression on PF-07799933 monotherapy. # indicates patient with *BRAF*^{V600E}+ primary brain tumor who achieved a confirmed PR after the data cutoff. Note: response categories are per RECIST 1.1 except for primary brain tumor, which is categorized by RANO. B, binimetinib combination; C, cetuximab combination; CR, complete response; PR, partial response; SD, stable disease; PD, progressive disease; NE, not evaluable; NCNP, non-CR/non-PD; p48, *BRAF* p48 splice variant; gain, *BRAF* copy number gain.

(right)]. PF-07799933 treatment also caused regressions of subcutaneously implanted *BRAF*^{G469A} (Class II)-mutant NSCLC, *BRAF*^{K601E} (Class II)-mutant melanoma and *BRAF* indel-mutant pancreatic cancer tumors [Fig. 1D (left)]. In contrast, plixorafenib was less efficacious against *BRAF*^{V600E}- and *BRAF*^{G469A}-mutant models, consistent with less *in vitro* pERK inhibition and known *in vivo* metabolic vulnerability (23, 33). Similarly, consistent with less *in vitro* pERK inhibition, exarafenib was less active against the *BRAF*^{V600E}-mutant model [Fig. 1C (left)]. For plixorafenib and exarafenib, we confirmed exposures achieved in animals approximated those achieved in humans (Supplementary Fig. S3A and S3B). Thus, the observed decreased efficacy relative to PF-07799933 ± binimetinib was not due to decreased exposures relative to clinically achievable doses in humans. In a *BRAF*^{V600}-mutant melanoma patient-derived xenograft (PDX) model harboring an acquired *BRAF* p61 splice variant, the combination of encorafenib + binimetinib did not improve the minimal antitumor activity of binimetinib monotherapy. However, single agent PF-07799933 demonstrated superior activity, and its combination with binimetinib further augmented efficacy, resulting in tumor regression, while remaining well-tolerated without body weight loss [Fig. 1D (right)].

In summary, these data indicate that PF-07799933 is a brain-penetrant, selective, pan-mutant BRAF inhibitor. PF-07799933 inhibited pERK *in vitro* in cells driven by *BRAF*^{V600E}-mutant monomers, BRAF Class II/III-mutant dimers, and treatment-acquired genetic alterations that induce

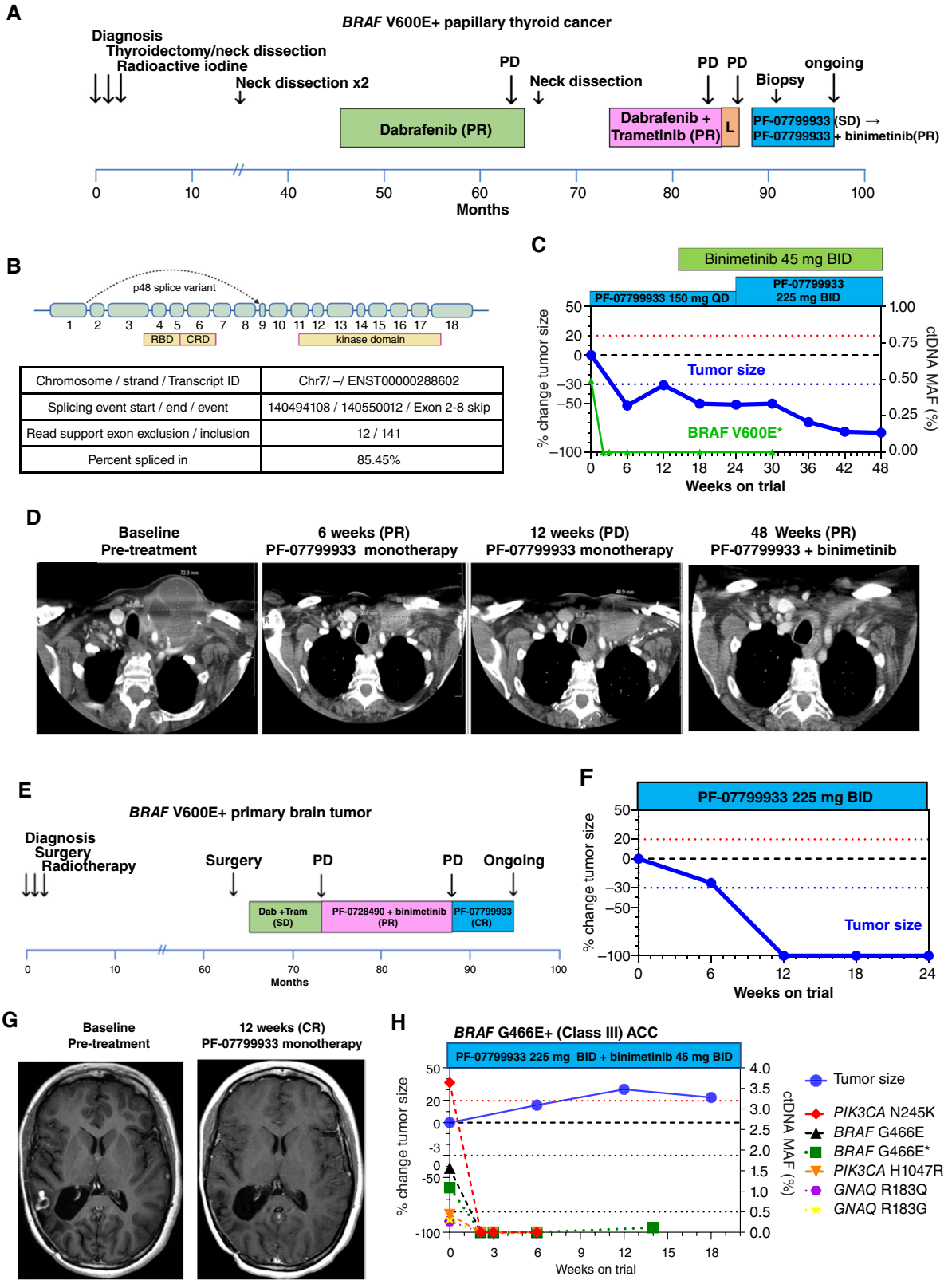

Chromosome / strand / Transcript ID	Chr7/ –/ ENST00000288602
Splicing event start / end / event	140494108 / 140550012 / Exon 2-8 skip
Read support exon exclusion / inclusion	12 / 141
Percent spliced in	85.45%

Figure 4. PF-07799933 overcomes *de novo* and acquired resistance and intracranial progression in patients with *BRAF*-mutant cancer. **A,** Previous therapies (best overall response to each systemic therapy shown in parenthesis) and timing of lymph node biopsy that showed a p48 splice variant for a patient with *BRAF*^{V600E}+ papillary thyroid cancer. **B,** Structure of the *BRAF* p48 in-frame *BRAF* splice-variant detected by tumor mRNA analysis. The table shows details of the spliced mRNA identified in 15% of all *BRAF* transcripts in a biopsy sample with 13% V600E MAF (*continued on following page*)

mutant-*BRAF*^{V600E} dimerization. Furthermore, PF-07799933 disrupted endogenous mutant-*BRAF*:wild-type-*CRAF* dimers in cells containing *BRAF*^{V600E} + p61 splice variant or *BRAF*^{V600E} + *NRAS*^{Q61K} that induce mutant *BRAF* dimerization. However, PF-07799933 spared pERK and did not disrupt *BRAF*-wild-type:*CRAF*-wild-type dimers *in vitro* in *BRAF* wild-type cells. Finally, PF-07799933 had broad *in vivo* antitumor activity, systemically and in the brain, against *BRAF*^{V600E} and non-V600 mutant proteins as monotherapy, and against *BRAF*^{V600E} with a treatment-acquired *BRAF* p61 splice variant in combination with binimetinib.

Characteristics of the Patients

From August 2022 to July 2023, 30 patients with *BRAF*-mutant solid tumors at nine centers in the United States and Canada were treated with PF-07799933 at 50 mg QD (n = 4 monotherapy), 150 mg QD [n = 4 monotherapy, n = 4 + binimetinib, n = 4 + cetuximab (all colorectal cancer, CRC)], 225 mg BID (n = 5 monotherapy, n = 4 + binimetinib), and 450 mg BID (n = 5 monotherapy; Supplementary Table S3). Tumor types were melanoma (n = 13/43%), CRC (n = 5/17%), primary brain (n = 4/13%), thyroid (n = 3/10%), and breast adenoid cystic carcinoma (ACC), salivary gland adenocarcinoma, cholangiocarcinoma, esophageal squamous carcinoma, and NSCLC (n = 1/3% each). *BRAF* mutations were Class I (V600E; 22/73%), Class II (4/13%), and Class III (4/13%). All patients with *BRAF*^{V600E}-mutant cancers were previously treated with an approved BRAF inhibitor regimen [n = 8/22 (36%) ≥2 lines; Supplementary Table S3]. All patients eligible for an immune checkpoint inhibitor (ICI) for an approved indication (including all patients with *BRAF*^{V600E}-mutant melanoma) also received previous treatment with an ICI (Supplementary Table S3).

PK-Informed Dose Escalation Enables Rapid Achievement of Therapeutic PF-07799933 Dose

Traditional first-in-patient phase 1 dose escalation designs enroll patients in fixed dose levels of a single anticancer drug based on observed toxicities (DLT). This risks underdosing many patients early on who cannot benefit because the dose is suboptimal and prevents potential benefit from rationally selected combination partners. Therefore, we developed a flexible approach that considered both observed toxicity and actual drug exposures to determine the amount of each dose increase (Fig. 2A).

First, we defined safe steady-state C_{max} and AUC_{tau} in patients based on the nonclinical toxicology of PF-07799933 (see "Methods"). Next, we limited each allowable dose increase to 2×, with the actual dose increase determined by the Bayesian logistic regression model (BLRM)/escalation with overdose control (EWOC) model based on the DLT rate. However, if no DLTs were observed, and the ratios of nonclinical steady-state C_{max} and AUC_{tau} to the values observed in patients were >40 in ≥2/3 patients, the dose increase could be 3×. This margin of exposure (MOE) and lower-than-required starting dose (50 mg QD) maximized patient safety and were possible due to the preclinical potency and pharmaceutics properties of PF-07799933 (Supplementary Methods). We also allowed intraparticipant dose escalation and/or rational addition of binimetinib or cetuximab (for patients with CRC) after progression on PF-07799933 monotherapy or, for combination, with PF-07799933-related toxicity known to be ameliorated by combination ("Methods"; ref. 34).

No DLTs were observed, and steady-state C_{max}/AUC_{tau} MOEs for each of the first two dose levels (50 mg QD, 150 mg QD) were >40 in 2/3 treated patients (Fig. 2B). This enabled sequential threefold dose increases across the first three dose levels (50 mg QD → 150 mg QD → 225 mg BID) for a ninefold increase in total daily dose. PF-07799933 achieved drug concentrations in patients at 225 mg BID (dose level 3) that exceeded inhibitory concentrations for multiple *BRAF* mutants based on the cell-based pERK assay for the duration of the dosing interval, and approximated concentrations associated with 30 mg/kg QD dosing in mice (Fig. 2C).

Although no DLTs occurred at 225 mg BID, MOEs were <40 for all patients, limiting the next dose increase to twofold (i.e., 450 mg BID). At this dose, PF-07799933 showed high interpatient PK variability and lower exposures in 3/4 patients than for patients treated at 225 mg BID, likely due to dose-limited absorption (Supplementary Fig. S4). Therefore, this dose was not investigated further and a new formulation is being introduced (see Discussion).

Efficacy

Efficacy according to investigator assessments as of August 24, 2023, for 28 patients with measurable disease at baseline and ≥1 post-baseline imaging assessment who initiated PF-07799933 as monotherapy (n = 16, 6 added binimetinib sequentially per protocol, see Methods) or in combination with binimetinib (n = 8) or cetuximab (n = 4, all CRC) is summarized in Fig. 3A and Supplementary Fig. S5A. All patients were refractory to standard systemic therapies, and all patients with *BRAF*^{V600E}-mutant cancers previously received approved BRAF inhibitor treatments (Supplementary Table S3).

For 20 patients with *BRAF*^{V600}-mutant cancers who initiated treatment with PF-07799933 monotherapy (n = 12, 3 added binimetinib) or combination with binimetinib (n = 5) or cetuximab (n = 3, all CRC), overall response rate (ORR) increased with PF-07799933 starting dose from 50 mg QD to 225 mg BID: 0/3 responses by RECIST 1.1 or RANO at 50 mg QD, 1/7 at 150 mg QD, and 4/7 at 225 mg BID, including one complete response (CR; Fig. 3A). A fifth patient (with BRAF inhibitor-refractory *BRAF*^{V600E} + primary brain tumor)

Figure 4. ***(Continued)*** (Supplementary Table S5), likely representing the acquisition of the splice variant in cis in all V600E transcripts. **C,** Change in the sum of longest tumor diameters of target lesions (blue, normalized to baseline) and in *BRAF*^{V600E} ctDNA (green). Note: ctDNA assay cannot detect splice variants in mRNA. Imaging for weeks 36 to 48 was obtained after the data cutoff. **D,** Images of a large left neck target lesion mass during treatment. **E,** Previous therapies for a patient with a *BRAF*^{V600E}+ primary brain tumor. PF-07284890 is an investigational, brain-penetrant BRAF monomer inhibitor. **F,** Change in the sum of target lesion diameters (no ctDNA was detected in this patient). **G,** Images of a right temporal lobe target lesion during treatment. **H,** Change in the sum of the longest tumor diameters and mutations detected in ctDNA for a patient with *BRAF*^{G466E}-mutant ACC. * indicates *BRAF*^{V600E} or *BRAF*^{G469A} detected with *BRAF* gene-specific ctDNA assay. ACC, adenoid cystic carcinoma; CR, complete response; PR, partial response; SD, stable disease; PD, progressive; L, lenvatinib; MAF, mean allele frequency.

treated with 225 mg BID + binimetinib [latter added for PF-07799933 monotherapy-related adverse event (AE) per protocol] achieved an ongoing, confirmed partial response after the data cutoff. There were 0/3 responses at 450 mg BID, a dose limited by variable and low PK as described above. Efficacy was observed across tumor types. The median duration of treatment was 3.5 months (range 0.5–12.9). The median duration of response was not reached (range 2.8+, NE), and 4/5 responders remained on treatment and in response as of the data cutoff (Fig. 3B).

Two patients are summarized in detail in Fig. 4. First, a patient with BRAF inhibitor-refractory *BRAF*^{V600E}-mutant thyroid cancer with a *BRAF* p48 splice variant experienced ongoing, sustained tumor reduction up to −80% (consistent with a confirmed PR) upon the addition of binimetinib, after experiencing an unconfirmed partial response (PR) followed by PD on PF-07799933 150 mg QD monotherapy (Fig. 4A–D). Sustained efficacy in combination with binimetinib was consistent with preclinical *in vivo* efficacy experiments in a splice variant-containing model and may result from more sustained inhibition of MAPK signaling in the tumor cells [Fig. 1D (right); see "Discussion"]. Second, a patient with a *BRAF*^{V600E}-mutant primary brain tumor refractory to two lines of BRAF + MEK inhibitors experienced an ongoing confirmed CR with PF-07799933 225 mg BID monotherapy (Fig. 4E–G).

Among eight patients with *BRAF* Class II (n = 4) or Class III (n = 4) mutations treated with PF-07799933 monotherapy (n = 4, 3 added binimetinib) or combination with binimetinib (n = 3) or cetuximab (n = 1, CRC), there were no responses (Supplementary Fig. S5A). However, only one patient received PF-07799933 treatment at a dose of 225 mg BID and in combination with binimetinib. This patient, with treatment-refractory, *BRAF* G466E (Class III)–mutant breast ACC, with previous progression on seven lines of systemic therapy and without acceptable alternative treatment options, experienced clinical improvement and a molecular CR in ctDNA despite radiographic PD, and remains on treatment beyond PD, as permitted by protocol (Fig. 4H; Supplementary Fig. S5B; see "Discussion").

Safety

PF-07799933 was well-tolerated as monotherapy or combination. There were no DLTs and the MTD was not reached; ≥1 treatment-emergent AE (TEAE) with monotherapy and combination occurred in 94% and 100% of patients, respectively, and was grade ≥3 in 28% and 44%, respectively. TEAEs reported in ≥3 patients regardless of attribution are shown in Supplementary Table S4. The most common TEAEs for monotherapy were fatigue (any grade 44%/grade ≥3 0%), headache (28%/0%), vision blurred [22%/6% (a single patient with grade 3)], and lipase increased (16%/0%). The most common TEAEs for combinations were peripheral edema (33%/0%), acneiform rash, diarrhea, and fatigue (each 28%/0%). A single patient treated with PF-07799933 at 450 mg BID monotherapy had their dose reduced for AEs of vision blurred, peripheral sensory neuropathy, myalgia, fatigue, and decreased appetite. 6/8 AEs of blurred vision resolved without dose modification, and there were no abnormal findings reported on repeat ophthalmic examinations. No patient discontinued treatment for a study drug-related AE.

DISCUSSION

Although approved BRAF monomer inhibitors (in combination with MEK or EGFR inhibitors) have transformed treatment for patients with *BRAF*^{V600}-mutant cancer, long-term efficacy is limited by adaptive reactivation of ERK signaling, resistance from BRAF dimer formation in tumor cells, and poor brain penetration. Investigational pan-RAF dimer inhibitors overcome resistance preclinically, but many require intermittent dosing and dose modifications that may limit clinical activity and combinability (14, 15, 17–19). Recently, the pan-RAF dimer inhibitor tovorafenib dosed once weekly was associated with durable responses in pediatric patients with *BRAF* fusion+ or *BRAF*^{V600E}+ low-grade glioma (35). However, efficacy was lower in patients with recent prior MAPK inhibitor treatment and in patients with other tumor types, and treatment was still associated with frequent dose reductions and interruptions due to toxicities from pan-RAF inhibition (16, 35–37). Although the selective BRAF dimer inhibitor plixorafenib overcomes some liabilities preclinically, it requires codosing with cobicistat, which may limit combinability with MEK inhibitors and other drugs that are also metabolized by CYP3A4 (21–23).

PF-07799933 was developed to address all of these liabilities. Here, we present preclinical experiments that confirmed significant inhibition of pERK in *BRAF*-mutant cells, significant sparing of pERK in *BRAF* wild-type cells, and combinability with a MEK inhibitor. PF-07799933 monotherapy demonstrated strong antitumor activity, systemically and in the brain, against *de novo BRAF*^{V600E} (Class I) and non-V600E *BRAF* (Class II, III, or indel) mutant tumors and, in combination with binimetinib, against a *de novo BRAF*$^{V600E-}$ + acquired *BRAF* p61 splice variant mutant tumor.

Traditional phase 1 trials would have explored PF-07799933 monotherapy with a dose escalation design that only considered observed toxicity. This strategy was necessary in an era when most anticancer treatments were nonspecific, toxic, and often only modestly effective. However, for a highly specific agent against a credentialed oncogenic target, it risks exposing many patients to subtherapeutic doses early on and ineffective monotherapy later. Therefore, we implemented a novel, safety- and PK-guided dose escalation design that enabled rapid achievement of an efficacious dose, early intrapatient dose escalation, and early rational combination (Fig. 2). The AE profile of PF-07799933 was generally similar, but of lower grade, to that of approved BRAF inhibitors, and the lack of DLTs allowed for two sequential threefold dose increases across the first three dose levels. In particular, AEs of blurred vision as seen with approved BRAF and MEK inhibitors were primarily of low grade, without findings on ophthalmic examinations, and most resolved without dose modification. This safety profile, along with contemporaneous PK profiling, accelerated dose escalation to quickly achieve evidence of clinical activity in patients with *BRAF*^{V600E}–mutant solid tumor, systemically and in the brain, after failure of approved BRAF + MEK inhibitors, and in the presence of acquired resistance mutations. To our knowledge, this includes the first evidence of efficacy in a patient with a *BRAF* splice variant (Fig. 4A–D). Although the total number of patients is small, PF-07799933 at 225 mg BID ± binimetinib achieved an ORR of 57% (4/7, not including a fifth patient with confirmed response after data cutoff) for patients with BRAF

inhibitor-refractory patients with $BRAF^{V600E}$ solid tumors. This response rate compares favorably to that of exarafenib [ORR = 17% (1/6), at its recommended dose for expansion of 300 mg BID], and of plixorafenib + cobicistat [ORR 18% (3/17)], in similar patient populations (14, 23).

There are limitations to this study. The small number of patients and heterogeneous use of combination treatment may complicate comparisons to other RAF inhibitors. We have not yet observed tumor responses in patients with *de novo BRAF* Class II or III non-V600 mutations (no indel patients have been enrolled) despite clear monotherapy antitumor activity against *BRAF* Class II and indel-mutant mouse tumor xenografts *in vivo* at clinically achievable exposures of PF-07799933 [Fig. 1D (left)]. However, few patients with *BRAF* non-V600 have been enrolled to date, with only one having received PF-07799933 at an efficacious dose of 225 mg BID and in combination with binimetinib. This patient achieved a molecular ctDNA CR despite radiographic PD and has continued ongoing treatment for clinical benefit beyond PD (Fig. 4H). For some patients, it is possible that co-occurring driver mutations in the setting of Class II and Class III *BRAF* mutations blunt antitumor efficacy [e.g., *MYB-NUMB* fusion, *PIK3CA* H1047R in the patients with G466E (Class III) + ACC with a molecular CR; Supplementary Fig. S5A; Supplementary Table S5]. For *BRAF* Class II/III expressing tumors, it is important to note that reports of the clinical activity for other investigational BRAF or pan-RAF inhibitors have been limited. For example, 17 patients with Class II *BRAF* fusion+ have been treated with plixorafenib, with a reported ORR of 8% (1/13 evaluable); similarly, only three Class II patients were reported to have been treated with exarafenib, yielding an ORR of 33% (1/3; refs. 14, 23). Although PF-07799933 concentrations necessary for preclinical inhibitory were higher for *BRAF* non-V600- than $BRAF^{V600}$-mutant cancers, exposures achieved at 225 mg BID were consistent with significant pan-*BRAF* non-V600 target inhibition from preclinical data and provided higher pan-mutant *BRAF* target coverage than exarafenib or plixorafenib (Fig. 2C; Supplementary S3A and S3B). Upfront combination with a MEK inhibitor in additional patients and/or further dose escalation may provide even greater target coverage to address such Class II/III mutations clinically.

Increased exposures of PF-07799933 would take advantage of its favorable safety profile to drive enhanced target coverage and clinical efficacy. However, the decreased PK with high interpatient variability at a dose above 225 mg BID suggests that the initial formulation is likely affected by dose-limited absorption. A new formulation has been developed that preclinically overcomes this constraint, and preliminary clinical data indicate that this formulation may achieve higher exposures (Supplementary Fig. S4).

PF-07799933 monotherapy inhibited pERK and disrupted mutant-*BRAF*:wild-type-*CRAF* dimers in $BRAF^{V600E}$ + p61 splice variant+ melanoma cells in short-term assays *in vitro* (Fig. 1A and B). However, sustained tumor regression in the corresponding *in vivo* model and in a patient with *BRAF* V600E+ thyroid cancer harboring a *BRAF* p48 splice variant required combination with binimetinib [Figs. 1D (right) and 4A–D]. Efficacy across those tumors with distinct genotypes, RAF isoform levels, or resistance mechanisms, perhaps driving increased levels of RAF/MAPK signaling (including through additional RAF dimers) may require significant inhibition of RAF/MAPK signaling in the tumor cells. We have shown that this may be achieved at tolerable PF-07799933 doses in combination with binimetinib.

Despite permitting rational combination with binimetinib or cetuximab after PD on PF-07799933 monotherapy, some patients may not be able to receive sufficient combination treatment due to clinical deterioration.

Finally, current tumor response evaluation criteria do not account for sequential combination–dependent antitumor activity. This is exemplified by the patient with $BRAF^{V600E}$ + p48 splice variant+, who despite experiencing an ongoing −80% decrease in tumor size (relative to baseline imaging) after the addition of binimetinib, is considered to have a best overall response of SD by RECIST 1.1 due to prior PD on PF-07799933 monotherapy (Fig. 4A–D).

In summary, PF-07799933 demonstrated proof-of-concept antitumor activity, tolerability, and combinability in patients with *BRAF*-mutant cancers using a novel first-in-human phase 1 trial design that incorporated flexible dose escalation based on safety and rapid PK in patients. This included substantial tumor reductions in patients previously treated with approved BRAF inhibitor therapies (and other approved agents), with drug-acquired resistance mutations, and with brain involvement. Future development will more fully evaluate PF-07799933 as an upfront combination with a MEK inhibitor in patients with *BRAF* V600- and non-V600-mutant cancers with prior progression on approved targeted treatments.

METHODS

Preclinical Characterization of PF-07799933 Activity

Cell Lines, Xenografts, and Animal Care. All cells were obtained from ATCC except for A375-luciferase (Creative Biogene), WM3629 (Rockland), and MEL21514 (see below). All cell lines were cultured according to the recommended guidelines for the parental lines and used for experimentation within six passages. Efficacy studies with the CTG-1441 and CTG-0362 PDX models were performed at Champions Oncology. The MEL21514 PDX was generated from a biopsy provided by a female Hispanic patient with melanoma (51 years of age) following a relapse from Braftovi and Mektovi treatment (MT Group). $BRAF^{V600E}$ mutation and p61 splice variant expression in the MEL21514 PDX tumor were confirmed by whole-exome sequencing and RNA sequencing, respectively (Genewiz). For cell line development, MEL21514 PDX tumor samples were dissociated using the Miltenyi Biotec Human Tumor Dissociation Kit in combination with the gentleMACS Octo Dissociator according to the suggested hard tumor protocol. The dissociated cell suspension was then magnetically labeled with the Miltenyi Mouse Cell Depletion Kit and separated using the MACS Magnetic Separator for the enrichment of human tumor cells. Isolated MEL21514 tumor cells were pooled and established in culture using Renaissance Essential Tumor Medium/RETM (Rockland Inc.) supplemented with 10% fetal bovine serum/FBS (Hyclone), penicillin/streptomycin and cholera toxin. Following 10 passages in RETM, MEL21514 cells were grown in RPMI, supplemented with 10% FBS and 1-mmol/L sodium pyruvate. Cell lines and PDXs were authenticated by short tandem repeat profiling and regularly evaluated for *Mycoplasma* and murine viruses (MycoAlert, Lonza, Inc.; IDEXX; Charles River Research Animal Diagnostic Services).

All procedures performed on animals were in accordance with regulations and established guidelines and were reviewed and approved by Pfizer's Institutional Animal Care and Use Committee. All mice were

obtained at 6 to 8 weeks of age (Envigo), housed in groups of 5, and allowed a 1-week acclimation period before cancer cell inoculation. Food, water, temperature, and humidity were maintained per Pharmacology Testing Facility performance standards in accordance with the 2011 Guide for the Care and Use of Laboratory Animals (NRC) and AAALAC-International. For subcutaneous xenografts, each cell line (5×10^6 cells) or PDX (cell suspension prepared with Miltenyi gentleMACS) was injected subcutaneously into the right flank of female *Foxn1*^{nu} mice and allowed to grow to approximately 200 mm^3 prior to randomization by tumor size into dosing groups of eight animals. Body weight and subcutaneous tumor volume [determined by the formula (length × width^2)/2] were recorded twice weekly. For intracranial xenografts, the A375-luciferase cell line (10,000 cells) was injected 2 mm lateral to the bregma at the bone suture line of female *Foxn1*^{nu} mice, with randomization after 7 days into dosing groups of ten animals based on tumor burden measured by total luminescence flux (photons/second) with an IVIS Spectrum *In Vivo* Imaging System (Perkin Elmer). Body weight and total flux were recorded twice weekly, with average total flux plotted against the day posttumor implantation.

Quantitative pERK Cell Analysis. Cells were seeded at 5×10^4/well into clear, black-bottom, 96-well plates, incubated overnight at 37°C, and incubated for 1 hour with a nine-point dilution series of each inhibitor, followed by 3.7% formaldehyde fixation, methanol permeabilization, costaining with pERK and GAPDH antibodies, costaining with goat secondary antibodies conjugated to IRDye 800CW (for pERK) or IRDye 680RD (for GAPDH), and analysis of staining intensity by in-cell Western assay (LI-COR Odyssey). Signal intensity for pERK was normalized to GAPDH and the DMSO-treated control samples to generate percent of control (POC) data, which were then plotted versus compound concentration using GraphPad Prism 9 software to generate IC_{50} data using a four-parameter curve fit. See Supplementary Table S6 for sources of primary antibodies.

Isothermal Stability Shift Dose Response Assays. Trypsinized A375 cell pellets were resuspended in PBS and treated with DMSO or PF-07799933 (concentrations ranging from 0.122 to 2,000 nmol/L) for 30 minutes at 37°C. Cells were heated to 50°C for 3 minutes in a PCR plate using a PTC-200 thermal cycler (MJ Research) and then promptly spun at 4,700 rpm in a swinging bucket centrifuge for 30 seconds at 4°C. Cells were lysed with three cycles of freeze–thawing in liquid nitrogen prior to adding nondenaturing buffer [10-mmol/L Na_2PO_4, 1.8-mmol/L KH_2PO_4 (pH 7.4), 137-mmol/L NaCl, 2.7-mmol/L KCl, 1-mmol/L $CaCl_2$, 10-mmol/L $MgCl_2$, 0.02% n-dodecyl β-D-maltoside, 2× complete protease inhibitor (Sigma), and 2% phosphatase inhibitor cocktails 2 and 3 (Sigma)]. Samples were sonicated using the Bioruptor water bath sonicator (Diagenode) for 15 seconds with 30 seconds rest for 10 cycles. Proteins were denatured and cysteine residues reduced and alkylated at 95°C for 10 minutes in 50 mmol/L 4-(2-hydroxyethyl)-1-piperazineethanesulfonic acid (pH 8.0), 1% SDS, 1% Triton-X-100, 1% NP-40, 1% Tween 20, 1% sodium deoxycholate, 5-mmol/L EDTA, 50-mmol/L NaCl, 1% glycerol, 10-mmol/L tris(2-carboxyethyl)phosphine, and 40-mmol/L chloroacetamide. Protein sample clean-up was achieved using the SP3 bead method with Sera-Mag SpeedBeads (GE Healthcare), and proteins were digested with trypsin and Lys-C at 37°C for 15 hours. Individual peptide samples were labeled using isobaric Tandem Mass Tag labeling (TMTpro 16plex), combined, desalted (Waters Oasis HLB cartridge), and high pH reverse-phase fractionation was performed prior to liquid chromatography–mass spectrometry analysis.

Peptides were fractionated by direct injection on an Ionopticks Aurora Ultimate column (1.7 µm, 0.075 mm × 250 mm) at 0.2 µL/minute using an UltiMate 3000 RSLCnano System (Thermo Scientific). Mobile phases used were (A) 0.1% formic acid aqueous and (B) 0.1% formic acid acetonitrile. Peptides were gradient eluted from 2% to 5% B in 5 minutes, 5% to 30% B in 95 minutes, and 30% to 95% B in 4 minutes. Mass spectrometry analysis was performed using an Orbitrap Eclipse (Thermo Scientific). Samples were run in positive ion mode with a source spray of 1,800 V and an ion transfer tube temperature of 300°C. MS1 scans were performed in the Orbitrap mass analyzer set to a mass range of 350 to 1,800 m/z at a resolution of 120,000 and an automatic gain control target of 1×10^6, normalized to 250%. MS2 fragmentation spectra were acquired using higher energy collision dissociation mode at 28% collision energy and a 1-m/z isolation window using the quadrupole. TMT 16plex reporter ions were quantified using the SPS MS3 method using higher energy collision dissociation fragmentation, multi-notch isolation, and a 2-m/z MS2 isolation window. MS3 spectra were acquired in the Orbitrap mass analyzer at 60,000 full width at half maximum resolution, a target of 1×10^5, normalized to 300%, and 118 milliseconds max fill time. Protein quantification data were extracted from the ProteinGroups.txt file generated by MaxQuant (v2.1.1.0) processing of all raw files. MS2 spectra were searched using a Uniprot human database downloaded June 6, 2022, allowing for two missed cleavages with trypsin/P and LysC/P proteolytic specificity, and using variable modifications set as methionine oxidation and N-terminal protein acetylation, and fixed modifications set as cysteine carbamidomethylation. Search tolerances were set to 10 ppm for MS1 precursor ions and 20 ppm for MS2 fragment ions. Protein and peptide level false discovery rate thresholds were set to 1%, and at least one unique or razor peptide was required for protein identification, and unique plus razor peptides were used for protein quantification. Concentration–response curves were fit with R code adapted from the R package, TPP2D, ProteinGroups.txt table generated by MaxQuant.

Co-Immunoprecipitation and Immunoblotting. For co-immunoprecipitations of endogenous RAF proteins, MEL21514 or A375-*NRAS*^{Q61K} cells were plated at 1.5×10^7 cells per 150-mm dish. Cells were incubated at 37°C, 5% CO_2 with DMSO vehicle control or indicated concentrations of encorafenib or PF-07799933 for 1 hour. Cell lysates were harvested in 1 mL per dish of magnesium lysis buffer [25-mmol/L 4-(2-hydroxyethyl)-1-piperazineethanesulfonic acid pH 7.5, 75-mmol/L NaCl, 5-mmol/L $MgCl_2$, 5% glycerol, and 0.1% NP-40] supplemented with HALT protease/phosphatase inhibitor cocktail (Pierce). Lysates were clarified by centrifugation and normalized for protein concentration using the BCA assay kit (Pierce). Lysates were incubated with either BRAF (CST #53745) or CRAF (CST #14814) rabbit polyclonal antibodies at 1:100 dilution overnight at 4°C followed by incubation with protein-A conjugated magnetic beads (Dynabeads, Thermo Inc.) for 90 minutes at room temperature (22 °C). Protein immunoprecipitates were collected by magnetic separation and washed 3× with magnesium lysis buffer followed by resuspension in 1× LDS Sample Buffer (Thermo Inc.). Proteins were separated by SDS-PAGE using 4% to 20% NuPage gradient gels followed by transfer onto polyvinylidene difluoride membrane using the iBlot2 system. Membranes were incubated with indicated antibodies (see Supplementary Table S6) overnight at 4°C and imaged using enhanced chemiluminescence with West-Pico reagent (Pierce) on a Bio-Rad ChemiDoc XR imaging system. Immunoblot images were processed using Bio-Rad Image Lab and Adobe Illustrator software applications.

For co-immunoprecipitations of exogenous, wild-type RAF proteins, HEK293T cells grown in 100-mm dishes were transiently transfected with pcDNA3 vectors to enable cytomegalovirus promoter-driven expression of N-terminal fusions of GFP or V5-tagged human BRAF or CRAF; 48 hours posttransfection, cells were treated at indicated drug concentrations for 1 hour and processed as above.

BRAF Kinase Domain Protein Production, Crystallization, and Structure Determination. Long and short forms of N-terminal hexahistidine-tagged BRAF kinase domain BRAF-KD_L (residues 432–726) and BRAF-KD_S (residues 445–723 with three-point mutations F776A, R671A, and Y673A for solubility improvement) were

expressed in insect cells. The proteins were purified by Talon affinity and Resource S ion exchange chromatography. Fractions containing BRAF were applied to Superdex 200 size exclusion chromatography columns preequilibrated with two column volumes of sizing buffer (25-mmol/L NaH_2PO4/Na_2HPO4 pH 7.0, 100-mmol/L NaCl, 1-mmol/L tris(2-carboxyethyl)phosphine, 0.25% CHAPS, and 15% glycerol). The elution fractions were assessed by 4% to 20% gradient SDS-PAGE, and fractions containing pure BRAF protein were pooled and concentrated to 11 mg/mL by Amicon Spin concentrator (MWCO: 10,000) before flash-freezing and storage at −80°C.

Cocrystallization was performed by mixing an equal volume of the BRAF KD_S: encorafenib complex and reservoir solution, which consists of 18% PEG3350, 0.2-mol/L Na_2SO_4, 0.1-mol/L sodium–potassium phosphate, pH 6.6 with the hanging-drop vapor diffusion method. For BRAF-KD_L: PF-07799933 complex crystallization, the reservoir solution contains 17% PEG5000MME, 1% PEG6000, sodium acetate, 0.2-mol/L NaCl, and 5% Tacsimate. Both crystals were harvested and flash-frozen in liquid nitrogen in a reservoir solution containing 20% (v/v) glycerol as a cryoprotectant.

Diffraction data were collected at the in-house Rigaku FRE or FRX rotating anode X-ray generators equipped with Pilatus 1-mol/L or Eiger 4-mol/L photon counting detector. Image processing and data reduction utilized iMosflm from the CCP4 package or Rigaku CrysPro software package. The initial phasing maps were computed by molecular replacement in PHASER (38) using the atomic coordinates from the isomorphous crystal of the BRAF kinase domain (PDB ID code 4MNE) as the search model. The initial atomic positions and B factors of compound-bound BRAF-KD structures were refined by successive rounds of rigid body, real-space, and B factor refinements using PHENIX (39). Encorafenib and PF-07799933 were located in SIGMA-A weighted difference $mF_o - DF_c$ omit maps computed with phases from the refined models. Atomic models were then further refined by iterative manual model rebuilding into a sigma-weighted $2m|F_o| - D|F_c|$ map in COOT (40) and subsequent refinement cycles using PHENIX. Noncrystal symmetry refinement was used for the PF-07799933-bound BRAF-KD_L structure. Water molecules were added progressively in the later stages of refinement. Diffraction and refinement statistics are summarized in Supplementary Table S2.

Trial Oversight

The first-in-human phase 1 trial of PF-07799933 (NCT05355701) was designed and is overseen by sponsor representatives and the investigators and is supported by the sponsor. The FDA and Institutional Review Boards from each site approved the trial, and each patient provided written informed consent. Part 1 monotherapy dose escalation and Part 2 combination dose escalation with binimetinib or cetuximab are reported here.

Patients

Key inclusion criteria were age ≥16, treatment-refractory advanced/metastatic solid tumors, $BRAF^{V600}$ (Class I)/non-V600 (Class II/III) alteration in tumor and/or blood by local Clinical Laboratory Improvements Amendments laboratory test, Eastern Cooperative Oncology Group Performance Status 0 to 2, adequate end-organ function, and asymptomatic brain involvement if present. Symptomatic brain involvement was allowed once the dose of PF-07799933 achieved steady-state trough concentrations (C_{trough}) consistent with *BRAF* mutant inhibition based on nonclinical data. Key exclusion criteria were other active malignancy, major surgery or whole-brain irradiation within 4 weeks, hemodynamically unstable thromboembolism within 12 weeks, history of retinal vein occlusion, positive pregnancy test, uncontrolled infection, significant cardiovascular disease, active condition affecting drug absorption, ongoing other anticancer or prohibited concomitant medication, and previous treatment with a BRAF dimer inhibitor.

Trial Procedures

Patients received continuous, oral, once (QD) or twice daily (BID) PF-07799933 in 21-day cycles. Dose escalation utilized a BLRM guided by the EWOC principle. A dose could only be used if the risk of excessive toxicity >0.33 was <25%; ≥2 DLT–evaluable participants were required per cohort.

No dose increase between dose levels could normally exceed more than twofold the current dose level. However, if exposures resulted in sufficient safety margins [i.e., the ratio of steady-state maximum concentration (C_{max}) and area-under-the-curve-over-dosing-interval (AUC_{tau}) in the most sensitive nonclinical toxicology species (rat) at the severely toxic dose in 10% of animals (STD_{10}), to steady-state C_{max} and AUC_{tau} in ≥2/3 participants at a given dose level, was >40] and no DLTs were observed at the current and prior dose levels, the dose increase could be up to threefold over.

A participant could have PF-07799933 dose escalation or specific, rational combination therapy added [binimetinib for non-CRC or cetuximab for CRC] if (i) the dose to be escalated to or combined was allowed by BLRM/EWOC and he/she (ii) received ≥2 cycles of the current dose, (iii) experienced no AE meeting DLT criteria, and (iv) demonstrated disease progression by imaging, or (v) was experiencing a BRAF inhibitor AE ameliorated by the combination agent (e.g., skin rash, hyperkeratosis, and squamous cell carcinoma). Both intraparticipant dose escalation (including more than once) and combination addition were allowed, based on investigator preference, but each had to be done one at a time, with relevant criteria met each time.

Dose modifications and interruptions followed a prescribed algorithm. AEs were graded using Common Terminology Criteria for Adverse Events version 5.0. The response was evaluated by CT or MRI imaging using RECIST version 1.1 every 6 weeks (RANO for primary brain tumors).

Blood/plasma samples were collected prior to treatment and at defined intervals for PF-07799933 plasma concentration determination. ctDNA was prepared and analyzed using next-generation sequencing for the $BRAF^{V600}$ mutation (Sysmex) or G360 73-gene panel (v 2.10, Guardant Health). DNA and RNA were extracted from formalin-fixed, paraffin-embedded tumor samples and analyzed by Tempus xT.V4 (for DNA) and Tempus RNA.v2 (for RNA).

See Supplementary Data for additional details on the rationale for starting dose and dose escalation approach, PK analysis, and molecular analysis.

Outcome

The primary endpoints for Part 1 and Part 2 are first-cycle DLTs, AEs, lab, exam, and vital sign abnormalities, dose modifications, and recommended dose for expansion. Secondary endpoints include PK parameters, ORR by RECIST 1.1 (RANO for primary brain tumors), and duration of response. Exploratory outcomes include changes in ctDNA mutations.

Statistical Analysis

There is no formal hypothesis testing. Data are summarized descriptively.

Data Availability

Upon request, and subject to review, Pfizer, Inc. will provide the data that support the findings of this study. Subject to certain criteria, conditions, and exceptions, Pfizer, Inc. may also provide access to the related individual deidentified participant data. See https://www.pfizer.com/science/clinical-trials/trial-data-and-results for more information.

Authors' Disclosures

R. Yaeger reports grants and personal fees from Mirati Therapeutics; grants from Pfizer, Boehringer Ingelheim, and Daiichi Sankyo; personal fees from Zai Lab, Loxo@Lilly, and Revolution Medicine;

grants from Boundless Bio; and personal fees from Amgen outside the submitted work. M.A. McKean reports grants from Aadi Biosciences, Alpine Immune Sciences, Arcus Biosciences, Arvinas, Ascentage Pharma Group, ASCO, Astellas, Aulos Bioscience, Bayer, Bicycle Therapeutics, BioMed Valley Discoveries, BioNTech, Boehringer Ingelheim, Bristol Myers Squibb, C4 Therapeutics, Daiichi Sankyo, Dragonfly Therapeutics, EMD Serono, Epizyme, Erasca, Exelixis, Foghorn Therapeutics, G1 Therapeutics, Genentech/Roche, Gilead Sciences, GlaxoSmithKline, IconoVir Bio, IDEAYA Biosciences, Ikena Oncology, ImmVira Pharma, Infinity Pharmaceuticals, Jacobio Pharmaceuticals, Jazz Pharmaceuticals, Kechow Pharma, Kezar Life Sciences, Kinnate BioPharma, Krystal Biotech, MedImmune, Mereo BioPharma, and Metabomed; grants and other support from Moderna; grants from NBE Therapeutics, Nektar, Novartis, NucMito Pharmaceuticals, OncoC4, Oncorus, OnKure, and PACT Pharma; grants and other support from Pfizer; grants from Plexxikon, Poseida, Prelude Therapeutics, Pyramid Biosciences, Regeneron, Remix Therapeutics, Sapience Therapeutics, Scholar Rock, Seattle Genetics, Synthrox, Takeda Pharmaceuticals, Teneobio, Tempest Therapeutics, Tizona Therapeutics, TMUNITY Therapeutics, TopAlliance Biosciences, and Xilio; and other support from Castle Biosciences, Iqvia, and Merck outside the submitted work. R. Haq reports grants and other support from Pfizer during the conduct of the study. J.T. Beck reports grants from Pfizer outside the submitted work. M.H. Taylor reports personal fees from BMS, Eisai, Blueprint Medicines, Array BioPharma, Merck, Exelixis, Genzyme, Incyte, and Regeneron outside the submitted work. J.E. Cohen reports personal fees from Roche, Medison Pharma, Merck, AstraZeneca, and Bristol Myers Squibb outside the submitted work. D.W. Bowles reports nonfinancial support from Pfizer during the conduct of the study and personal fees from Exelixis outside the submitted work. S.M. Gadgeel reports personal fees from AstraZeneca, Pfizer, Takeda, Mirati, Novartis, Bristol Myers Squibb, Genentech/Roche, Glaxo, Janssen, Merck, Esai, Arcus, Blueprint Medicines, Lilly, Regeneron, Gilead, Amgen, Bayer, Esai, and Boehringer Ingelheim outside the submitted work, as well as and AstraZeneca—Member of IDMC of a Phase III trial Merck—Travel support to attend and present at a medical conference and Mirati-Travel support to attend and present at a medical conference. C. Mihalcioiu reports grants from Pfizer and personal fees from Pfizer outside the submitted work. K.P. Papadopoulos reports other support from Pfizer during the conduct of the study, as well as other support from Abbvie, Amgen, Anheart Therapeutics, AstraZeneca, Bayer, Bicycle Therapeutics, Biontech, CytomX Therapeutics, Daiichi Sankyo, Debiopharm, F-Star, Linnaeus Therapeutics, Mirati Therapeutics, Bristol Myers Squibb, Tempest Therapeutics, Treadwell Therapeutics, Lilly, Kezar Life Sciences, Monte Rosa Therapeutics, PharmaMar, Revolution Medicine, Sensei Biotherapeutics, Storm Therapeutics, Regeneron, Incyte, and Merck outside the submitted work. E.L. Diamond reports nonfinancial support from Pfizer, Inc., during the conduct of the study and personal fees from Opna Bio outside the submitted work. K.B. Sturtz reports other support from Pfizer during the conduct of the study. G. Feng reports as an employee of and a shareholder in Pfizer, Inc. T.-C. Mou reports personal fees and other support from Pfizer during the conduct of the study and personal fees and other support from Pfizer outside the submitted work and is an employee of Pfizer. S. Gadal reports grants from Pfizer during the conduct of the study. N. Rosen reports grants from Pfizer-Array during the conduct of the study; personal fees and other support from Beigene; personal fees from MAPCure; and grants from Revolution Medicine, AstraZeneca, and Chugai outside the submitted work; in addition, N. Rosen has a patent for Biomarkers of ERK inhibition issued. J.J. Gaudino reports a patent for WO2021250521 issued. P.A. Lee reports personal fees from Pfizer, Inc., outside the submitted work. S.M. Rothenberg reports other support from Pfizer, Inc., during the conduct of the study and other support from Pfizer, Inc., outside the submitted work. No disclosures were reported by the other authors.

Authors' Contributions

R. Yaeger: Data curation, supervision, investigation, writing–review and editing. **M.A. McKean:** Supervision, investigation, writing–review and editing. **R. Haq:** Supervision, investigation, writing–review and editing. **J.T. Beck:** Supervision, investigation, writing–review and editing. **M.H. Taylor:** Supervision, investigation, writing–review and editing. **J.E. Cohen:** Supervision, investigation, writing–review and editing. **D.W. Bowles:** Supervision, investigation, writing–review and editing. **S.M. Gadgeel:** Supervision, investigation, writing–review and editing. **C. Mihalcioiu:** Supervision, investigation, writing–review and editing. **K.P. Papadopoulos:** Supervision, investigation, writing–review and editing. **E.L. Diamond:** Data curation, formal analysis, investigation. **K.B. Sturtz:** Conceptualization, formal analysis, supervision, investigation, writing–review and editing. **G. Feng:** Data curation, formal analysis, investigation, project administration, writing–review and editing. **S.K. Drescher:** Formal analysis, investigation, writing–review and editing. **M.B. Reddy:** Conceptualization, supervision, writing–review and editing. **B. Sengupta:** Formal analysis, investigation. **A.K. Maity:** Formal analysis. **S.A. Brown:** Investigation. **A. Singh:** Formal analysis, supervision, investigation, writing–review and editing. **E.N. Brown:** Formal analysis, investigation. **B.R. Baer:** Formal analysis, investigation, writing–review and editing. **J. Wong:** Formal analysis, supervision, investigation, writing–review and editing. **T.-C. Mou:** Formal analysis, investigation, writing–review and editing. **W.-I. Wu:** Formal analysis, supervision, investigation, writing–review and editing. **D.R. Kahn:** Investigation. **S. Gadal:** Writing–review and editing. **N. Rosen:** Writing–review and editing. **J.J. Gaudino:** Supervision, investigation. **P.A. Lee:** Supervision, investigation, writing–review and editing. **D.P. Hartley:** Supervision, investigation, writing–review and editing. **S.M. Rothenberg:** Conceptualization, formal analysis, supervision, methodology, writing–original draft, project administration, writing–review and editing.

Acknowledgments

We thank Pfizer Boulder Research & Development, Array BioPharma, and Pfizer colleagues, including Nick Saccomano, Bin Li, Karyn Bouhana, Eric J. Hicken, Ellen R. Laird, Ray Li, William M. Old, Robb Van Gulick, and Jenn Winton. The study was funded by Pfizer, Inc. R. Yaeger was supported in part by the National Cancer Institute of the National Institutes of Health under award number P30 CA008748.

Note

Supplementary data for this article are available at Cancer Discovery Online (http://cancerdiscovery.aacrjournals.org/).

Received January 18, 2024; revised March 21, 2024; accepted April 26, 2024; published first May 1, 2024.

REFERENCES

1. Yao Z, Yaeger R, Rodrik-Outmezguine VS, Tao A, Torres NM, Chang MT, et al. Tumours with class 3 BRAF mutants are sensitive to the inhibition of activated RAS. Nature 2017;548:234–8.
2. Yao Z, Torres NM, Tao A, Gao Y, Luo L, Li Q, et al. BRAF mutants evade ERK-dependent feedback by different mechanisms that determine their sensitivity to pharmacologic inhibition. Cancer Cell 2015;28:370–83.
3. Nazarian R, Shi H, Wang Q, Kong X, Koya RC, Lee H, et al. Melanomas acquire resistance to B-RAF(V600E) inhibition by RTK or N-RAS upregulation. Nature 2010;468:973–7.
4. Poulikakos PI, Persaud Y, Janakiraman M, Kong X, Ng C, Moriceau G, et al. RAF inhibitor resistance is mediated by dimerization of aberrantly spliced BRAF(V600E). Nature 2011;480:387–90.

5. Long GV, Fung C, Menzies AM, Pupo GM, Carlino MS, Hyman J, et al. Increased MAPK reactivation in early resistance to dabrafenib/trametinib combination therapy of BRAF-mutant metastatic melanoma. Nat Commun 2014;5:5694.
6. Rizos H, Menzies AM, Pupo GM, Carlino MS, Fung C, Hyman J, et al. BRAF inhibitor resistance mechanisms in metastatic melanoma: spectrum and clinical impact. Clin Cancer Res 2014;20:1965–77.
7. Shi H, Hugo W, Kong X, Hong A, Koya RC, Moriceau G, et al. Acquired resistance and clonal evolution in melanoma during BRAF inhibitor therapy. Cancer Discov 2014;4:80–93.
8. Van Allen EM, Wagle N, Sucker A, Treacy DJ, Johannessen CM, Goetz EM, et al. The genetic landscape of clinical resistance to RAF inhibition in metastatic melanoma. Cancer Discov 2014;4:94–109.
9. Wagle N, Van Allen EM, Treacy DJ, Frederick DT, Cooper ZA, Taylor-Weiner A, et al. MAP kinase pathway alterations in BRAF-mutant melanoma patients with acquired resistance to combined RAF/MEK inhibition. Cancer Discov 2014;4:61–8.
10. Johnson DB, Menzies AM, Zimmer L, Eroglu Z, Ye F, Zhao S, et al. Acquired BRAF inhibitor resistance: a multicenter meta-analysis of the spectrum and frequencies, clinical behaviour, and phenotypic associations of resistance mechanisms. Eur J Cancer 2015;51:2792–9.
11. Kwong LN, Boland GM, Frederick DT, Helms TL, Akid AT, Miller JP, et al. Co-clinical assessment identifies patterns of BRAF inhibitor resistance in melanoma. J Clin Invest 2015;125:1459–70.
12. Kemper K, Krijgsman O, Kong X, Cornelissen-Steijger P, Shahrabi A, Weeber F, et al. BRAF(V600E) kinase domain duplication identified in therapy-refractory melanoma patient-derived xenografts. Cell Rep 2016;16:263–77.
13. Clark ME, Rizos H, Pereira MR, McEvoy AC, Marsavela G, Calapre L, et al. Detection of BRAF splicing variants in plasma-derived cell-free nucleic acids and extracellular vesicles of melanoma patients failing targeted therapy therapies. Oncotarget 2020;11:4016–27.
14. Spira A, Gambardella V, Kato S, Perez CB, Mckean M, Cao MG, et al. Abstract CT032: trials in progress: a global phase 1/1b clinical trial evaluating exarafenib (KIN-2787), a highly selective pan-RAF inhibitor, in adult patients with BRAF-altered solid tumors and NRAS mutant melanoma. Cancer Res 2023;83(8_Supplement):CT032.
15. Schram AM, Subbiah V, Sullivan R, Cosman R, Liu J, Sbar EI, et al. Abstract CT031: a first-in-human, phase 1a/1b, open-label, dose-escalation and expansion study to investigate the safety, pharmacokinetics, and antitumor activity of the RAF dimer inhibitor BGB-3245 in patients with advanced or refractory tumors. Cancer Res 2023;83(8_Supplement):CT031.
16. Rasco DW, Medina T, Corrie P, Pavlick AC, Middleton MR, Lorigan P, et al. Phase 1 study of the pan-RAF inhibitor tovorafenib in patients with advanced solid tumors followed by dose expansion in patients with metastatic melanoma. Cancer Chemother Pharmacol 2023;92:15–28.
17. Wolf J, Planchard D, Heist RS, Solomon B, Sebastian M, Santoro A, et al. 1387P Phase Ib study of LXH254 + LTT462 in patients with KRAS- or BRAF-mutant NSCLC. Ann Oncol 2020;31:S881–2.
18. Kim TW, Lee J, Shin SJ, Kim J-S, Kim YJ, Han HS, et al. Belvarafenib, a novel pan-RAF inhibitor, in solid tumor patients harboring BRAF, KRAS, or NRAS mutations: phase I study. J Clin Oncol 2019;37(15_suppl):3000.
19. Janku F, Iyer G, Spreafico A, Yamamoto N, Bang Y-J, Elez E, et al. A phase I study of LXH254 in patients (pts) with advanced solid tumors harboring MAPK pathway alterations. J Clin Oncol 2018;36(15_suppl):2586.
20. Yao Z, Gao Y, Su W, Yaeger R, Tao J, Na N, et al. RAF inhibitor PLX8394 selectively disrupts BRAF dimers and RAS-independent BRAF-mutant-driven signaling. Nat Med 2019;25:284–91.
21. Janku F, Vaishampayan U, Khemka V, Bhatty M, Zhang C, Hsu HH, et al. Abstract B176: results of a phase I study of PLX8394, a next-generation BRAF inhibitor, in refractory solid tumors. Mol Cancer Ther 2018;17(1_Supplement):B176.
22. de la Fuente M, Butowski N, Taylor J, Yaeger R, Tsai FY-C, Janku F, et al. CTNI-76. Efficacy of BRAF inhibitor plixorafenib (FORE8394) in recurrent, primary central nervous system tumors (pcnst). Neuro-Oncology 2023;25(Supplement_5):v95.
23. De La Fuente MI, Rodon JA, Yaeger R, Tsai FY-C, Janku F, Butowski NA, et al. Safety and efficacy of the novel BRAF inhibitor FORE8394 in patients with advanced solid and CNS tumors: results from a phase 1/2a study. J Clin Oncol 2023;41(16_suppl):3006.
24. Monaco KA, Delach S, Yuan J, Mishina Y, Fordjour P, Labrot E, et al. LXH254, a potent and selective ARAF-sparing inhibitor of BRAF and CRAF for the treatment of MAPK-driven tumors. Clin Cancer Res 2021;27:2061–73.
25. Suzuki R, Kitamura Y, Nakamura Y, Akashi H, Ogawa Y, Kawada H, et al. Anti-tumor activities of the new oral pan-RAF inhibitor, TAK-580, used as monotherapy or in combination with novel agents in multiple myeloma. Oncotarget 2020;11:3984–97.
26. Wang TS, Lee C, Severson P, Pelham RJ, Williams R, Miller NLG. Abstract 4927: exarafenib (KIN-2787) is a potent, selective pan-RAF inhibitor with activity in preclinical models of BRAF class II/III mutant and NRAS mutant melanoma. Cancer Res 2023;83(7_Supplement):4927.
27. Yen I, Shanahan F, Lee J, Hong YS, Shin SJ, Moore AR, et al. ARAF mutations confer resistance to the RAF inhibitor belvarafenib in melanoma. Nature 2021;594:418–23.
28. Chen SH, Zhang Y, Van Horn RD, Yin T, Buchanan S, Yadav V, et al. Oncogenic BRAF deletions that function as homodimers and are sensitive to inhibition by RAF dimer inhibitor LY3009120. Cancer Discov 2016;6:300–15.
29. Foster SA, Whalen DM, Ozen A, Wongchenko MJ, Yin J, Yen I, et al. Activation mechanism of oncogenic deletion mutations in BRAF, EGFR, and HER2. Cancer Cell 2016;29:477–93.
30. Poulikakos PI, Zhang C, Bollag G, Shokat KM, Rosen N. RAF inhibitors transactivate RAF dimers and ERK signalling in cells with wild-type BRAF. Nature 2010;464:427–30.
31. Joseph EW, Pratilas CA, Poulikakos PI, Tadi M, Wang W, Taylor BS, et al. The RAF inhibitor PLX4032 inhibits ERK signaling and tumor cell proliferation in a V600E BRAF-selective manner. Proc Natl Acad Sci U S A 2010;107:14903–8.
32. Heidorn SJ, Milagre C, Whittaker S, Nourry A, Niculescu-Duvas I, Dhomen N, et al. Kinase-dead BRAF and oncogenic RAS cooperate to drive tumor progression through CRAF. Cell 2010;140:209–21.
33. Sherman EJ, Tsai F, Janku F, Allen C, Yaeger R, Ammakkanavar NR, et al. 466P-efficacy of BRAF inhibitor FORE8394 in BRAF V600+ patients. Ann Oncol 2022;33:S197–224.
34. Drilon A, Sharma MR, Johnson ML, Yap TA, Gadgeel S, Nepert D, et al. SHP2 inhibition sensitizes diverse oncogene-addicted solid tumors to Re-treatment with targeted therapy. Cancer Discov 2023;13:1789–801.
35. Kilburn LB, Khuong-Quang D-A, Hansford JR, Landi D, van der Lugt J, Leary SES, et al. The type II RAF inhibitor tovorafenib in relapsed/refractory pediatric low-grade glioma: the phase 2 FIREFLY-1 trial. Nat Med 2024;30:207–17.
36. Rasco D, Olszanski AJ, Patnaik A, Espino G, Neuwirth R, Faucette S, et al. MLN2480, an investigational oral pan-RAF kinase inhibitor, in patients (pts) with relapsed or refractory solid tumors: phase I study. J Clin Oncol 2013;31(15_suppl):2547.
37. Olszanski AJ, Gonzalez R, Corrie P, Pavlick AC, Middleton M, Lorigan P, et al. Phase I study of the investigational, oral pan-RAF kinase inhibitor TAK-580 (MLN2480) in patients with advanced solid tumors (ST) or melanoma (MEL): final analysis. Ann Oncol 2017;28:v136–7.
38. McCoy A, Grosse-Kunstleve RW, Adams P, Winn M, Storoni L, Read R. Phaser crystallographic software. J Appl Crystallogr 2007;40:658–74.
39. Adams P, Afonine P, Bunkoczi G, Chen V, Davis I, Echols N, et al. PHENIX: a comprehensive Python-based system for macromolecular structure solution. Acta Crystallogr D Biol Crystallogr 2010;66:213–21.
40. Emsley P, Cowtan K. Coot: model-building tools for molecular graphics. Acta Crystallogr D Biol Crystallogr. 2004;60:2126–32.